Available online at www.sciencedirect.com
SCIENCE DIRECT®
Journal of Solid State Chemistry 177 (2004) 4013–4022
JOURNAL OF SOLID STATE CHEMISTRY
www.elsevier.com/locate/jssc

Structural homologies in benzylamino-*N*,*N*-bis methylphosphonic acid and its layered zirconium derivative

Riccardo Vivani[a,*], Ferdinando Costantino[a], Morena Nocchetti[a], Giacomo D. Gatta[b]

[a] *Dipartimento di Chimica, CEMIN, Centro di Eccellenza Materiali Innovativi Nanostrutturati, Università degli Studi di Perugia, via Elce di Sotto 8, 06123 Perugia, Italy*

[b] *Bayerisches Geoinstitut, Universität Bayreuth, Universität str. 30, D-95447 Bayreuth, Germany*

Received 3 June 2004; received in revised form 19 July 2004; accepted 22 July 2004
Available online 7 October 2004

Abstract

A new layered zirconium diphosphonate fluoride, $ZrF(O_3PCH_2)_2NHCH_2C_6H_5$ has been prepared and its structure determined ab initio by X-ray powder data and refined with the Rietveld method (orthorhombic, $a = 8.9429(2)$ Å, $b = 9.1746(2)$ Å, $c = 31.5654(7)$ Å, space group *Pbca*, $V = 2589.9(1)$ Å^3, $Z = 8$, $R_{wp} = 0.080$). Both phosphonic groups of each diphosphonate building block are bonded to zirconium atoms on the same side of each layer. Benzyl groups from adjacent layers are interdigitated in the interlayer region, with probable $\pi-\pi$ stacking interactions. The structure of the free benzylamino-*N*,*N*-bis methylphosphonic acid has been determined by single crystal X-ray data (monoclinic, space group $P2_1$, $a = 6.990(3)$ Å, $b = 5.635(2)$ Å, $c = 15.551(6)$ Å, $\beta = 92.930(3)^\circ$, $V = 611.7(4)$ Å^3, $Z = 2$, $R_1 = 0.072$, w$R_2 = 0.150$). As in the zirconium derivative, benzyl groups from adjacent layers are interdigitated and create a regular alternation of polar and non-polar regions.

Keywords: Ab initio structure solution; X-ray powder diffraction; Zirconium diphosphonates; Layered compounds; Functional solids

1. Introduction

Zirconium phosphonates have been widely investigated as a useful tool for material chemistry because they allow the preparation of tailor-made compounds, with structure and reactivity that can be tuned for specific purposes. They are very insoluble solids, and in most cases their structure can easily be predicted with good approximation, because it is often related to that of one of the main zirconium phosphate families, of α- or γ-type [1–4]. Therefore it is relatively easy to prepare a zirconium phosphonate with the desired framework structure, and bearing a specific functional group. However, many other original zirconium phosphonate structures have recently been reported, and it would be seen that research in this field is far from being exhausted [3,5,6]. *R*-amino-*N*,*N*-bis methylphosphonates (*R* = organic group) are versatile building blocks that have been used for the preparation of several metal(II) derivatives [7–15]. We recently reported the preparation and structural characterization of a series of new layered zirconium diphosphonates, in which *R* was an alkyl chain of various lengths, or a butanoic group [16,17]. These compounds showed similar structural features. Their layer framework consisted of corner sharing zirconium octahedra and phosphonate tetrahedra, so that the two phosphonic groups of the same diphosphonic unit were bonded on the same side of layers. Aminoalkyl groups pointed toward the interlayer regions from both sides of the inorganic layers. Alkyl chains bonded to adjacent layers were interdigitated.

In this work, the benzylamino-*N*,*N*-bis methylphosphonic group has been selected as the building block.

*Corresponding author. Fax: +39-075-585-5566.
E-mail address: ric@unipg.it (R. Vivani).

0022-4596/$ - see front matter © 2004 Elsevier Inc. All rights reserved.
doi:10.1016/j.jssc.2004.07.038

The structure of its zirconium derivative has been solved ab initio using X-ray powder diffraction data, and we have found that, despite a different crystal system and cell parameters, it is similar to that shown by the previous alkyl derivatives. In particular, this new compound shows the same layer framework and a similar interdigitated packing of organic groups in the interlayer region [16,17].

The structure of the diphosphonic acid has also been solved (by X-ray single crystal diffraction data) and is presented here. It shows an interesting supramolecular arrangement. Some features of its structure are also found in the zirconium derivative, and the comparison between these two structures allowed us to propose an explanation of some important differences found between this zirconium derivative and the other zirconium diphosphonates belonging to the same family.

2. Experimental

2.1. Synthesis procedures

Reagents: $ZrOCl_2 \cdot 8H_2O$ was a Merck Pro Analysi product. All the other chemicals were Carlo Erba RPE grade.

Synthesis of the diphosphonic acid: The benzylamino-*N*,*N*-bis methylphosphonic acid, of formula $(H_2O_3PCH_2)(HO_3PCH_2)NHCH_2C_6H_5$ (hereafter **1**) was synthesized according to the Moedritzer–Irani method [18]. After the synthesis, the diphosphonic acid, which was obtained as a white microcrystalline solid was purified by recrystallization using a water–ethanol mix as a solvent.

Synthesis of zirconium diphosphonate: Zirconium salt of **1**, of formula $ZrF(O_3PCH_2)_2NHCH_2C_6H_5$ (hereafter **2**) was prepared as follows: a clear solution containing 0.015 mol L^{-1} of $ZrOCl_2 \cdot 8H_2O$, 0.03 mol L^{-1} of **1** and 0.3 mol L^{-1} of hydrofluoric acid was prepared using a 1/1 (v/v) water–propanol mix as a solvent. The solution (0.118 L) was maintained in a closed plastic vessel at 80 °C until a white precipitate was formed (5–7 days). The precipitate was separated by centrifugation and washed three times with a 1/1 (v/v) water–propanol mixture. Finally it was dried in an oven at 70 °C. Anal. found: Zr, 22.50; P, 15.65; F, 4.85; N, 3.22; C, 26.35; H, 2.55%; Calcd. for $ZrP_2FO_6NC_9H_{12}$: Zr, 22.62; P, 15.41; F, 4.72; N, 3.48; C, 26.85; H, 2.98%.

2.2. Analytical procedures

The composition of **2** was determined as follows. Zirconium, phosphorus and fluorine contents were determined as ZrO_2, phosphates and fluorides, respectively, after sample mineralization. A 0.2 g portion of the sample was mixed with an excess of equimolar Na_2CO_3 and K_2CO_3 mixture, put in a ceramic vessel and gradually heated up to 800 °C in an oven. The calcined solid was then recovered with water, filtered through paper and washed to quantitatively transfer the soluble sodium and potassium phosphates formed into the washing water. Amounts of phosphate and fluoride in this washing solution were determined by ion chromatography. The residual filtered solid was washed with 0.1 M hydrochloric acid to dissolve the excess alkaline carbonates, then washed with water, and finally calcined to ZrO_2, which was determined gravimetrically.

Fluorine was also determined using an alternative method. About 0.1 g of sample was refluxed for 3 h with 10 mL of 1 M NaOH up to complete hydrolysis. After filtration and appropriate dilution, the solution was injected into the ion chromatographer.

2.3. Instrumental procedures

C, H and N elemental analysis was performed with a Carlo Erba 1106 Analyser.

Ion chromatography was performed with a Dionex series 2000 i/sp instrument, using an IonPack AS4A column and a buffer solution, of the following composition: 1.7×10^{-3} M in $NaHCO_3$, 1.8×10^{-3} M in Na_2CO_3 (3.5×10^{-3} M for fluoride ions) as an eluent.

Coupled thermogravimetric (TG) and differential thermal (DTA) analysis was performed with a Netzsch STA490C thermoanalyser under a 20 mL min^{-1} air flux with a heating rate of 5 °C min^{-1}.

FT-IR spectra of the solid samples were recorded under vacuum with a Bruker IFS 113 V spectrometer by the KBr pellet technique.

Single crystal diffraction data collection of **1** was carried out on an XCALIBUR Oxford Instruments diffractometer equipped with a CCD detector, at the Dipartimento di Scienze della Terra, University of Perugia, using graphite monochromated Mo$K\alpha$ radiation, and operating at 50 kV and 30 mA. To maximize the reciprocal space coverage, a combination of ω and φ scans was used, with a step size of 0.5° and a time of 30 s/frame. The distance between the crystal and the detector was 60.4 mm.

X-ray powder diffraction (XRD) patterns for structure determination and Rietveld refinement of **2** were collected according to the step scanning procedure with Cu$K\alpha$ radiation on a Philips X'PERT APD diffractometer, PW3020 goniometer equipped with a bent graphite monochromator on the diffracted beam. 0.5° divergence and scatter slits and a 0.1 mm receiving slit were used. The LFF ceramic tube operated at 40 KV, 30 mA. To minimize preferred orientations, the sample was carefully side loaded onto an aluminum sample holder with an oriented quartz monocrystal underneath. Further acquisition details are reported in Table 1.

Table 1
Crystal data and refinement details for **1** and **2**

Sample	**1**, single crystal	**2**, powder
Empirical formula	$C_9H_{15}NO_6P_2$	$ZrP_2FO_6NC_9H_{12}$
Formula weight	295.2	402.2
Crystal system	Monoclinic	Orthorhombic
Space group	$P2_1$	*Pbca*
a (Å)	6.990(3)	8.9429(2)
b (Å)	5.635(2)	9.1746(2)
c (Å)	15.551(6)	31.5654(7)
β (degree)	92.930(3)	
V (Å^3)	611.7(4)	2589.9(1)
Z	2	8
T (°C)	25	25
ρ_{calc} (g cm^{-3})	1.603	2.06
λ (Å)	0.71069	1.54056
μ (mm^{-1})	0.375	
F(000)	308	1600
2θ range for data collection (degree)	10–50	3.3–124.5
Step scan increment, 2θ (degree)		0.02
Step scan time (s)		30
Reflections collected, unique	3405, 1833	2061
R_{int}	0.084	
Data, parameters	1833, 162	6060, 98
GoF on F^2	0.963	
R_1[a], wR_2[b] [$I>4\sigma(I)$]	0.072, 0.150	
R_1[a], wR_2[b] (all data)	0.092, 0.160	
Largest diff. peak, hole (eÅ^{-3})	+0.457, −0.370	
R_p[c]		0.059
R_{wp}[d]		0.080
R_{F^2}[e]		0.047
χ[f]		4.55

[a] $R_1 = \Sigma(|F_{obs}|-|F_{calc}|)/\Sigma|F_{obs}|$.
[b] w$R_2 = [\Sigma[w(F^2_{obs}—F^2_{calc})^2]/\Sigma[w(F^2_{obs})^2]]^{0.5}$.
[c] $\Sigma-\Sigma$
[d] $\Sigma-\Sigma$
[e] $R_{F^2} = \Sigma|F_o^2 - F_c^2|/\Sigma|F_o^2|$
[f] $\chi = [\Sigma w(I_o - I_c)^2/(N_o - N_{var})]^{1/2}$

2.4. Structure determination and refinement for *1*

Most single crystals of **1**, prepared using different crystallization procedures, were found to be affected by severe twinning and mosaicity. After an accurate search, a prismatic crystal ($0.14 \times 0.12 \times 0.06$ mm) was selected as the best candidate for structural analysis. The structure was solved under the $P2_1$ space group using the direct methods implemented in the SIR97 program [19] and refined using a full matrix least-square method on F^2 with the SHELXL-97 package [20]. The carbon atoms of the aromatic ring (C(13) to C(18)) were restrained in an idealized planar ring with C–C bond lengths of 1.39 Å. Anisotropic thermal parameters were refined for all non-hydrogen atoms. Hydrogen atoms bonded to carbon atoms were added in calculated positions and were not refined. Hydrogen atoms bonded to oxygen and nitrogen atoms were located by difference Fourier maps. This assignment was then checked taking into account the P–O bond lengths and the molecular packing, as will be discussed later on. The position of hydrogens bonded to oxygen atoms was refined restraining O–H bond lengths at 0.93(2) Å. Isotropic displacement parameters of hydrogen atoms were set at a value 1.2 times higher than that of the corresponding atom (1.5 times for terminal oxygen atoms) and were not refined. Since the crystal contained twins, the TWIN routine, using the [−1 0 0/0 1 0/0 0 1] matrix, was used, within the SHELXL-97 package. Neutral atomic scattering factors were used, and a structure refinement performed using the ionic scattering curves did not provide significantly different results. Crystal data and details of the refinement are reported in Table 1.

2.5. Structure determination and refinement for *2*

Unit cell parameters were determined using both TREOR90 [21] and DICVOL91 [22] programs. For this, a preliminary peak-profile fitting, using pseudo-Voigt functions for the determination of the position of $K\alpha_1$ maxima, was carried out. Indexation gave the orthorhombic cell reported in Table 1 as the best solution [$M(20) = 17$] [23].

The analysis of the indexed pattern clearly revealed the presence of the following limiting reflection conditions: $hk0$, $h = 2n$; $h0l$, $l = 2n$; and $0kl$, $k = 2n$, which suggested *Pbca* as the probable space group. In addition, a systematic comparison of the number of peaks found and the number of possible peaks, in all orthorhombic space groups using the Chekcell program [24], estimated *Pbca* as the best choice.

The structure was solved in the direct space with a "Reverse Monte Carlo" method implemented in the FOX program [25]. The program is able to optimize a structural model described by the use of building blocks defined in terms of their internal coordinates, such as bond lengths, bond angles, and dihedral angles. Optimization was performed by comparing randomly generated configurations, using the "integrated R_{wp}" (iR_{wp}) as the cost function [25]. Trial structures were generated using the "Parallel Tempering" algorithm [26]. The structure was described using one ZrO_5F octahedron and one diphosphonate molecule as building blocks. Hydrogen atoms were omitted. Starting values for bond lengths and angles were taken from similar systems found in the literature, and constrained within a standard deviation of 0.15 Å and 10°, respectively. Benzyl ring lengths and angles were not optimized. All other dihedral angles were left to change freely. In short, (about 1 million trials, 20 min) the program found a stable configuration which was also geometrically sound, a connectivity similar to that previously observed

in analogous systems [16,17], and a sufficiently low iR_{wp} value (0.12). The model was then refined using the Rietveld method performed with the GSAS program [27]. Scale factor, background, zero shift, cell parameters and peak profile were first refined. Atomic parameters were then refined. All the atoms were refined isotropically and neutral atomic scattering factors were used. Thermal displacement parameters of heavy atoms (Zr and P) were refined independently, while those of light atoms (F, O, N, and C) were refined by constraining the program to apply the same shifts. The shape of the profile was modeled by a pseudo-Voigt function [28] (7 parameters) in which two parameters for asymmetry at low angle were included [29]. No correction was applied for preferred orientation and absorption. Stereochemical restraints were introduced for bond distances (2.03(3) Å for Zr–O, 1.95(3) Å for Zr–F, 1.54(3) Å for P–O, 1.85(3) Å for P–C, 1.52(3) Å for aliphatic C–C, 1.39(3) Å for aromatic C–C and 1.45(3) Å for C–N bonds) to avoid divergence in the first stages of refinement. The statistical weight of these restraints was decreased as the refinement proceeded, but it was not possible to set it to zero, due to some unrealistic light atom bond distances. At the end of the refinement, the shifts in all parameters were less than their standard deviations. Crystal data and details of the refinement are reported in Table 1.

Supplementary data (atomic positions and thermal parameters) for structures **1** and **2** are available as supporting informations. Crystallographic data (excluding structure factors) for these structures have been deposited with the Cambridge Crystallographic Data Centre as supplementary publication no. CCDC 229461 and 229462, respectively. Copies of the data can be obtained free of charge on application to CCDC, 12 Union Road, Cambridge CB2 1EZ, UK (fax: (44) 1223 336-033; e-mail: deposit@ccdc.cam.ac.uk).

3. Results

3.1. Structure description

3.1.1. $(H_2O_3PCH_2)(HO_3PCH_2)NHCH_2C_6H_5$ (1)

Fig. 1 shows the molecular packing of **1**, while Fig. 2 shows its asymmetric unit. Table 2 lists selected bond distances and angles for **1**.

The structure of **1** can be described as a supramolecular assembly of building units, that are arranged in interdigitated molecular layers, so that two regions, with two different chemical characters, can be identified within this structure.

PO_3H_2 groups from adjacent molecular layers face each other and create a strongly polar region. The two phosphonate groups per each formula unit are crystallographically and chemically non-equivalent. According to difference Fourier maps, the phosphonate group related to the P(2) atom is doubly protonated, on O(4) and O(6), while the phosphonate group related to P(1) bears only one hydrogen atom, that is bonded with O(9). Accordingly, the latter phosphonate group must be negatively charged. In line with this, the bond lengths of protonated P–O groups (average length = 1.527 Å) are longer than P(2)–O(5) and P(1)–O(8) terminal groups (average length = 1.469 Å). Even though the P(1)–O(3) bond length (1.519(5) Å) is similar to the other protonated groups, no hydrogen atoms have been found on O(3). This oxygen atom is probably negatively charged. The molecule shows a zwitterionic character, because a fourth hydrogen atom has been found on N(7), which results positively charged. This behavior is also shown in solution, as assessed by the titration curve of a solution of **1** with sodium hydroxide (Fig. 3). The curve shows a first inflexion point, at pH about 3.5 related to the neutralization of one strongly acidic proton per mol of **1**, and a second inflexion point at pH about 9.5 corresponding to two less acidic protons per mol of **1**. These data can be interpreted taking into account that the nitrogen atom is protonated by a phosphonate group. The inflexion point related to the proton bonded to the nitrogen atom cannot be detected under these conditions, due to its very low acidity. A number of hydrogen bonds (listed in Table 3) are formed between protonated P–OH and unprotonated P–O groups belonging to adjacent molecules. Additional lateral interactions between molecules within the same

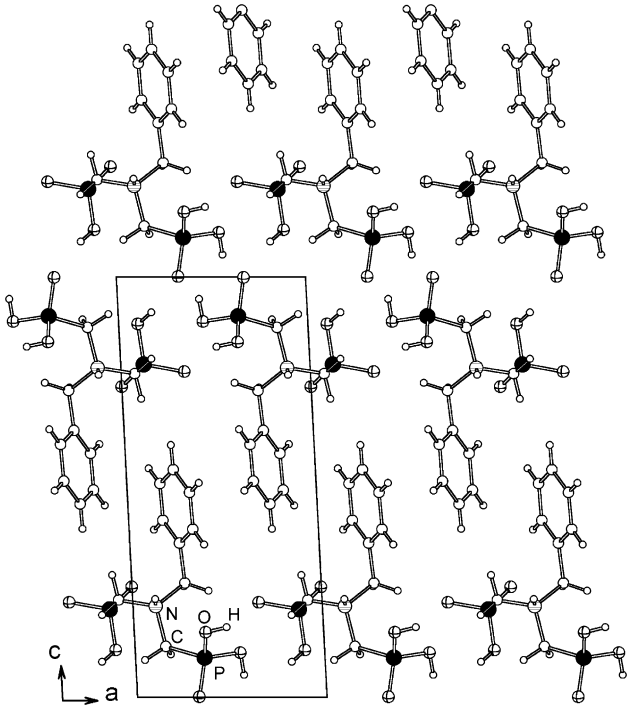

Fig. 1. Schematic view of the structure of **1** along the *b*-axis.

Table 2
Selected bond lengths and angles for **1**

Bond	Length (Å)	Angle	Amplitude (degree)
P(1)–O(3)	1.519(5)	O(8)–P(1)–O(3)	115.8(3)
P(1)–O(9)	1.539(6)	O(8)–P(1)–O(9)	112.3(4)
P(1)–O(8)	1.458(6)	O(3)–P(1)–O(9)	107.8(3)
P(1)–C(12)	1.850(10)	O(8)–P(1)–C(12)	112.1(4)
P(2)–O(6)	1.514(6)	O(3)–P(1)–C(12)	100.1(4)
P(2)–O(4)	1.527(7)	O(9)–P(1)–C(12)	107.9(4)
P(2)–O(5)	1.479(6)	O(5)–P(2)–O(6)	116.7(4)
P(2)–C(10)	1.824(8)	O(5)–P(2)–O(4)	109.6(3)
N(7)–C(12)	1.484(1)	O(6)–P(2)–O(4)	107.3(4)
N(7)–C(11)	1.513(1)	O(5)–P(2)–C(10)	103.4(4)
N(7)–C(10)	1.532(1)	O(6)–P(2)–C(10)	109.0(3)
C(11)–C(13)	1.520(8)	O(4)–P(2)–C(10)	110.8(4)
C–$C_{aromatic}$	1.390	C(12)–N(7)–C(11)	114.5(7)

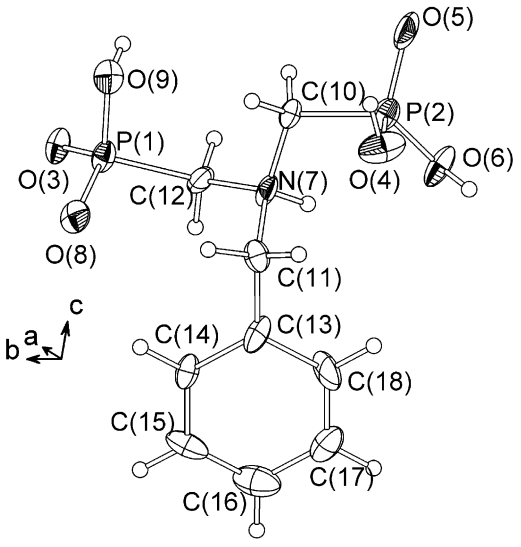

Fig. 2. Schematic view of asymmetric unit for **1**. Thermal displacement ellipsoids are drawn at the 50% probability level.

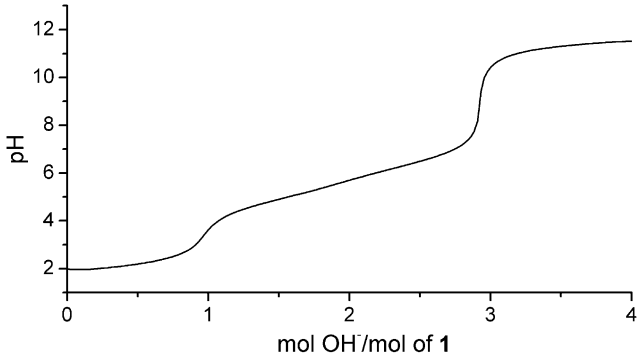

Fig. 3. Titration curve of a 0.02 M aqueous solution of **1** with 0.1 M NaOH.

molecular layers have been found. As usual for this kind of compounds [9,12,15–17], a hydrogen bond is present between N(7) and P–O(8)#2 (#2 = x, $y+1$, z). Furthermore, benzyl tails of adjacent molecular layers are interdigitated in a herringbone close packed arrangement, and define a non-polar layered region. Benzene ring planes are about 3.6 Å apart, and $\pi-\pi$ interactions are probably present between them. It is very likely that these lateral interactions cooperate to reinforce the cohesion of molecular layers. The presence of layered polar regions alternated with strongly interacting non-polar layers makes this compound of interest for applications in the field of ion exchange, intercalation, or proton conduction. Studies are in progress to test the possibility of operation within the polar region, for example by ion exchange or intercalation reactions, without the disruption of the whole structure.

3.1.2. $ZrF(O_3PCH_2)_2NHCH_2C_6H_5$ (2)

Fig. 4 shows the structure of **2**, while Fig. 5 shows its asymmetric unit. Table 4 lists selected bond distances and angles for **2**. Fig. 6 shows the final Rietveld and difference plot.

Structure **2** is similar to that previously described for aminopentyl and aminobutanoic derivatives [16,17]. However, some relevant differences can be ascribed to the different nature of the organic groups.

Structure **2** arises from the packing, along the *c*-axis, of hybrid inorgano-organic layers interacting by van der Waals forces. Each layer of **2** is made of corner sharing ZrO_5F octahedra and O_3PC tetrahedra. Zr octahedra are placed in two parallel planes about 4 Å apart. The octahedron axis defined by F(20)–Zr(1)–O(5)#1 bonds (#1 = $-0.5+x$, $0.5-y$, $1-z$) is tilted toward both *a* and *b* directions (see Fig. 5). Pairs of phosphonate tetrahedra, facing the same side of the layers, belong to the same diphosphonate moiety, and are bridged together by the benzylamino group, via the nitrogen atom. The two phosphonate groups of each diphosphonic unit are crystallographically and chemically non-equivalent, since one of them is triply connected to three zirconium

Table 3
Hydrogen bond lengths and angles for **1**

D–H···A bond	D–H length (Å)	H···A length (Å)	D···A length (Å)	DHA angle amplitude (degree)
O(6)–H(6)···O(3)#1	0.938(7)	1.616(7)	2.46(1)	147.5(6)
N(7)–H(7)···O(8)#2	0.910(6)	1.839(6)	2.68(1)	154.4(4)
O(9)–H(9)···O(5)#3	0.923(5)	1.870(8)	2.55(1)	128.7(5)
O(4)–H(4)···O(5)#4	0.931(6)	1.760(8)	2.59(1)	146.9(5)

Symmetry operations used to generate equivalent atoms: #1 = $x-1$, $y-1$, z; #2 = x, $y-1$, z; #3 = $-x+2$, $y+1/2$, $-z+2$; #4 = $-x+1$, $y+1/2$, $-z+2$.

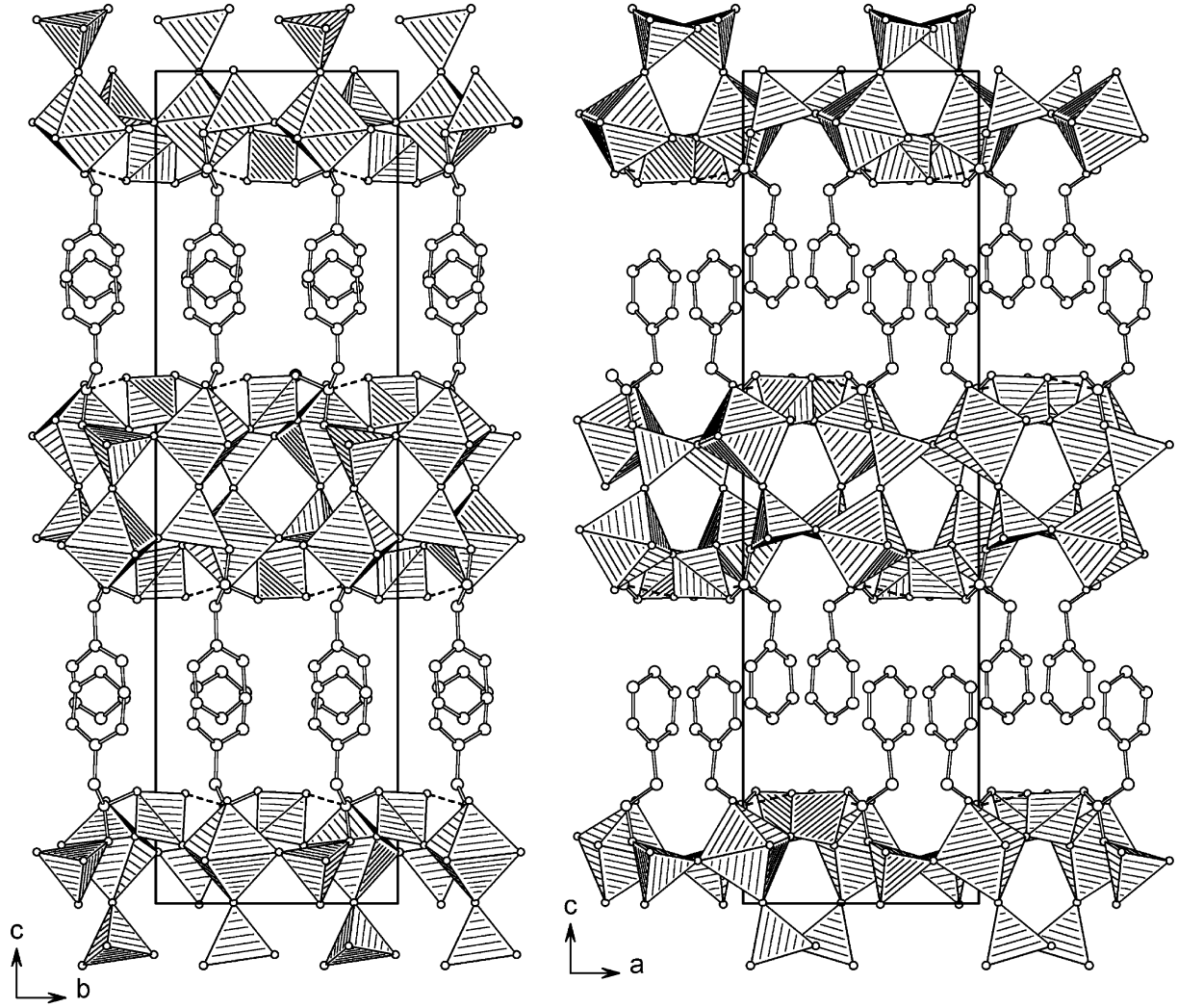

Fig. 4. Schematic view of the structure of **2**, viewed along the *a*-axis (left) and the *b*-axis (right). Zirconium and phosphorus coordination environments are represented as ZrO_5F octahedra and PO_3C tetrahedra, respectively. Hydrogen bonds between N(12) and O(9) are represented as dashed lines.

atoms, while the second one is connected by only two zirconium atoms. The third P–OH group points toward the nitrogen atom of an adjacent diphosphonic group. The N(12)···O(9)#5 distance (#5 = $1.5-x$, $0.5+y$, z) is only 2.48(1) Å (see Fig. 5), indicating that a strong hydrogen bond is present between them, or more probable, that the amino group is protonated by the phosphonate, as found in the pure diphosphonic acid structure, and in other similar systems [9,12,15]. This hypothesis is in agreement with IR spectrum of **2**, that shows a broad band in the region 2600–2200 cm^{-1} that may be due to $R_3N–H^+$ stretching vibration. In addition, no PO–H stretching bands are observed, and titration of the solid with NaOH did not detect any

acidic proton. This zwitterionic character was also identified in the other zirconium aminodiphosphonates belonging to the same family [16,17]. The conformation of the diphosphonic residue is very similar to that found for **1**, as evinced by comparing Figs. 2 and 5. Benzyl groups point toward the interlayer region from both sides of the layers and form a herringbone interdigitated arrangement with those coming from adjacent layers, as observed also in the pure diphosphonic acid structure (see Fig. 7). In this kind of layer framework, the free area associated with each R group is $a \times b/2 \simeq 41\,\text{Å}^2$, that is about two times the estimated cross section for a benzene ring. Similarly to results found for structure **1**, this interdigitated arrangement generates a close packing condition with the probable formation of $\pi-\pi$ interactions between benzyl groups, since benzene ring planes are about 3.5 Å apart. These interactions seem to be globally strong since the interlayer region appears to be inaccessible to guest species, and all our attempts of intercalation with several different molecules failed.

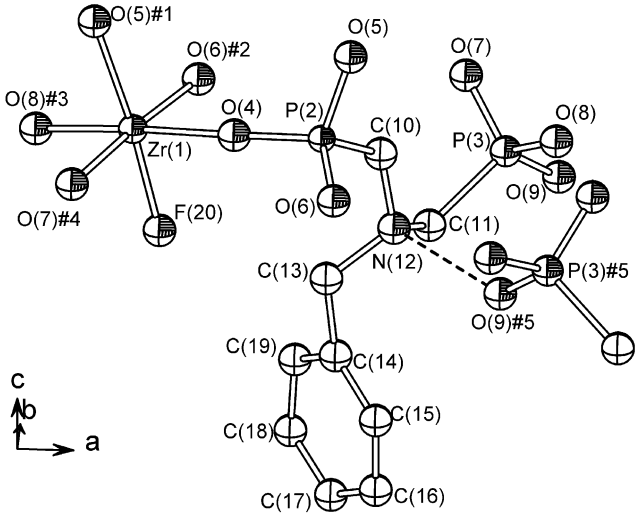

Fig. 5. Schematic view of the structure of **2** containing the asymmetric unit. Hydrogen bonds are represented as dashed lines. Thermal displacement spheres are drawn at the 50% probability level. Symmetry operations used to generate equivalent atoms: #1 = −0.5 + x, 0.5−y, 1−z; #2 = 0.5−x, 0.5 + y, z; #3 = −1 + x, y, z; #4 = 0.5−x, −0.5 + y, z; #5 = 1.5−x, 0.5 + y, z.

3.2. Thermal behavior

Fig. 8 shows the TG and DTA curves for **2**. Weight starts to be lost at about 350 °C, the temperature at which the organics start to decompose in more than one unresolved step. At the end of the analysis, at 1100 °C, only cubic zirconium pyrophosphate, ZrP_2O_7, was found. The total weight loss was 34.56%, in good agreement with the calculated value (34.10%).

3.3. FT-IR spectra

The IR spectra of **1** and **2** are shown in Fig. 9a and b, respectively. Spectrum of **1** shows some weak sharp bands over 3000 cm^{-1} (3027 and 3013 cm^{-1}), due to the aromatic C–H stretching vibrations, and more intense sharp peaks at 2988 and 2938 cm^{-1}, due to methylene C–H stretching vibrations. A broad absorption band in

Table 4
Selected bond lengths and angles for **2**

Bond	Length (Å)	Angle	Amplitude (degree)	Angle	Amplitude (degree)
Zr(1)–O(4)	2.076(6)	O(4)–Zr(1)–O(5)#1	96.7(4)	O(4)–P(2)–C(10)	108.5(7)
Zr(1)–O(5)#1	2.096(6)	O(4)–Zr(1)–O(6)#2	88.8(4)	O(5)–P(2)–O(6)	107.7(6)
Zr(1)–O(6)#2	2.112(6)	O(4)–Zr(1)–O(7)#4	90.4(4)	O(5)–P(2)–C(10)	104.4(5)
Zr(1)–O(7)#4	2.051(7)	O(4)–Zr(1)–O(8)#3	176.2(4)	O(6)–P(2)–C(10)	114.1(7)
Zr(1)–O(8)#3	2.054(7)	O(4)–Zr(1)–F(20)	87.4(4)	O(7)–P(3)–O(8)	109.0(6)
Zr(1)–F(20)	1.932(6)	O(5)#1–Zr(1)–O(6)#2	94.07(34)	O(7)–P(3)–O(9)	111.0(6)
P(2)–O(4)	1.563(7)	O(5)#1–Zr(1)–O(7)#4	89.4(4)	O(7)–P(3)–C(11)	108.2(7)
P(2)–O(5)	1.596(6)	O(5)#1–Zr(1)–O(8)#3	87.0(4)	O(8)–P(3)–O(9)	108.0(6)
P(2)–O(6)	1.546(7)	O(5)#1–Zr(1)–F(20)	175.3(4)	O(8)–P(3)–C(11)	110.2(6)
P(2)–C(10)	1.804(8)	O(6)#2–Zr(1)–O(7)	176.5(4)	O(9)–P(3)–C(11)	110.5(6)
P(3)–O(7)	1.501(7)	O(6)#2–Zr(1)–O(8)	89.7(4)	P(2)–C(10)–N(12)	119.2(8)
P(3)–O(8)	1.518(7)	O(6)#2–Zr(1)–F(20)	88.3(4)	P(3)–C(11)–N(12)	118.1(8)
P(3)–O(9)	1.554(8)	O(7)#4–Zr(1)–O(8)	90.9(4)	C(10)–N(12)–C(11)	109.2(9)
P(3)–C(11)	1.850(8)	O(7)#4–Zr(1)–F(20)	88.2(4)	C(10)–N(12)–C(13)	116.3(10)
C(10)–N(12)	1.373(9)	O(8)#3–Zr(1)–F(20)	89.02(35)	C(11)–N(12)–C(13)	107.2(8)
C(11)–N(12)	1.466(9)	O(4)–P(2)–O(5)	111.5(6)	N(12)–C(13)–C(14)	118.0(12)
N(12)–C(13)	1.453(9)	O(4)–P(2)–O(6)	110.6(6)		
C(13)–C(14)	1.500(8)				
O(9)#5···N(12)	2.48(1)				

Symmetry operations used to generate equivalent atoms: #1 = −0.5 + x, 0.5−y, 1−z; #2 = 0.5−x, 0.5 + y, z; #3 = −1 + x, y, z; #4 = 0.5−x, −0.5 + y, z; #5 = 1.5−x, 0.5 + y, z.

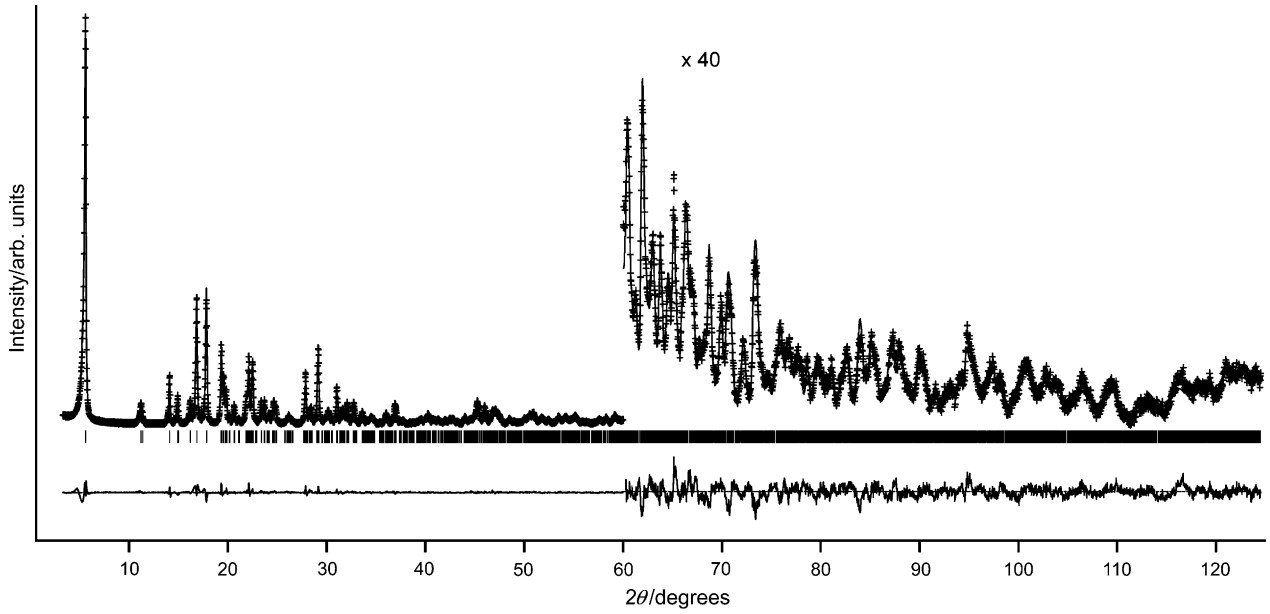

Fig. 6. Final Rietveld and difference plot for **2**.

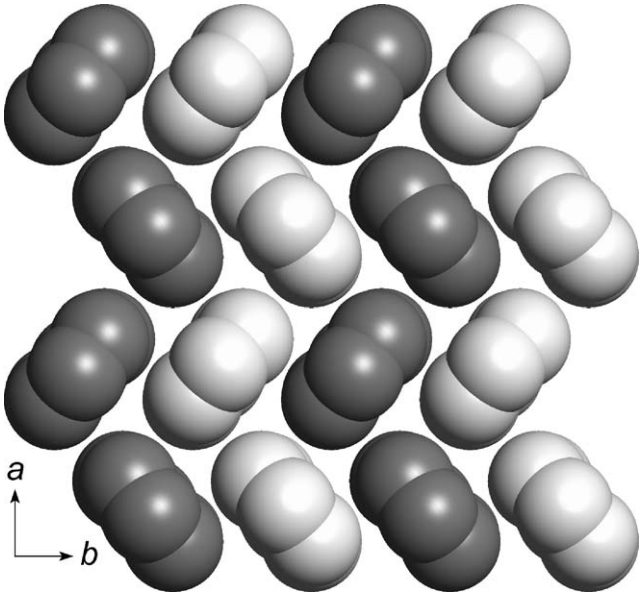

Fig. 7. View of a slice of the interlayer region for **2**, along the *c*-axis, showing the close packed arrangement of benzyl groups. Benzyl groups coming from adjacent layers are represented in different gray intensities. Van der Waals radii of carbon atoms are set at 1.55 Å.

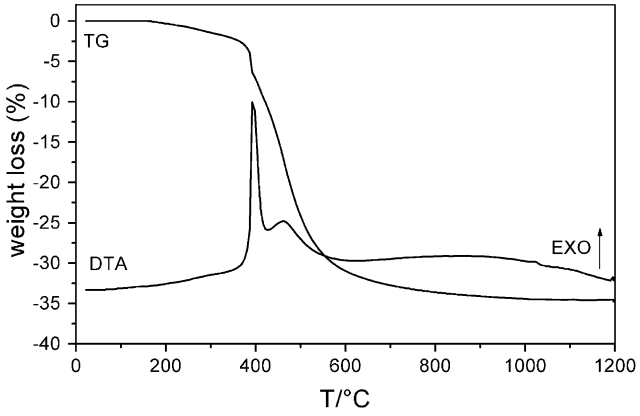

Fig. 8. TG and DTA curves for **2**.

the 3000–2400 cm^{-1} region is associated to the stretching vibrations of O–H bonds which are involved in H-bonds. Superimposed to this, a second broad band may be also present in the region 2600–2200 cm^{-1}, due to the R_3N–H^+ stretching vibration, which is typical for this kind of compounds [17], and is also observed in the zirconium derivative (Fig. 9b). Absorption bands in the range 1500–1400 cm^{-1} are due to C–C stretching vibrations of the aromatic ring, while below 1400 cm^{-1} a complex system of bands, attributable to P–O stretching and bending modes, and to C–C and C–H bending vibrations, is observed. Different from **1**, the IR spectrum of **2** does not show PO–H vibration bands, while C–H stretching (2985 and 2940 cm^{-1}) and aromatic C–C stretching bands (around 1450 cm^{-1}) are still found. Also in this case, the large band, well evident in the region 2600–2200 cm^{-1}, may be due to the R_3N–H^+ stretching vibration. Below 1400 cm^{-1} the complex system of bands can be ascribed to the vibrations of the rest of the framework, especially P–O stretching and bending modes.

4. Discussion

The structure of **2** is similar to that of aminopentyl and aminobutanoic derivatives [16,17] for many

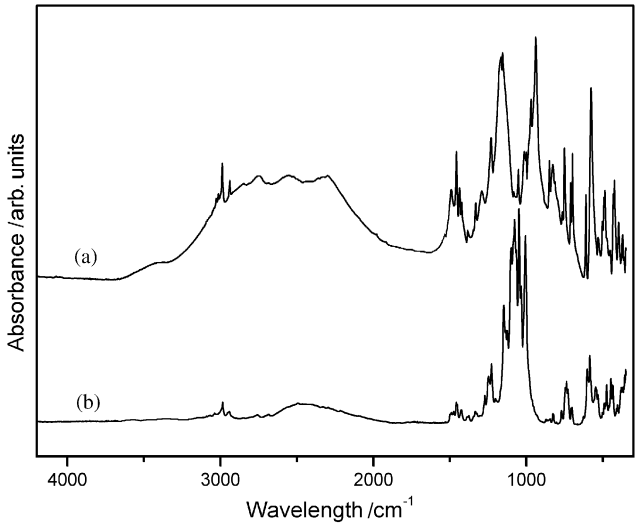

Fig. 9. FT-IR spectra of **1** (curve a) and **2** (curve b).

features, such as the atomic connectivity inside the inorganic layers, the interdigitated arrangement of the interlayer organic groups, their zwitterionic character. However, the *b*-axis of **2** is considerably shorter than the corresponding axis (the *c*-axis) in the previously described compounds (9.1746(2) Å for **2**, 10.9793(3) Å for the aminopentyl and 10.7924(4) Å for the aminobutanoic derivative), while the *a*-axis of **2** is close to *b*-axis of the other two structures (8.9429(2) Å vs. 8.8723(3) and 8.9900(4) Å, respectively). Furthermore, the benzylamino derivative structure is stretched along the *c*-axis, perpendicular to the layer plane, with a larger thickness of zirconium planes (4 Å vs. 2.2 Å) and an unusually large value of Zr(1)–O(5)#1–P(2)#1 angle [178.6(7)°, $\#1 = -0.5 + x$, $0.5 - y$, $1 - z$].

One hypothesis that may explain these differences originates from steric requirements and reciprocal interactions of benzyl groups. We can assume that for **1**, which is a molecular solid, its $a \times b$ value (about 78.4 Å^2) is determined by the steric requirements for obtaining a close packed arrangement of benzyl groups. Since this area contains four interdigitated benzyl groups, a free area of about 19.6 Å^2 is associated with each benzyl group. A very similar $a \times b$ value (about 82.1 Å^2), and consequently a free area of about 20.5 Å^2 per organic group, has been found for **2**. These values are very different from the $b \times c$ value of about 97.4 Å^2 and the area associated to each alkyl chain (24.8 Å^2) for the aminopentyl derivative. From these data we may conclude that the structure of **2** is compressed in a direction parallel to the layers in order to find the best contact and the most favorable energetic conditions for the interlayer benzyl groups. As a consequence of this, the inorganic part of the structure, that is the layer framework, is expanded along a direction perpendicular to the layers, and the structure is stretched along the *c*-axis. On the contrary, in the alkyl derivatives the best reciprocal interlayer contacts are probably simply found by a conformational change of alkyl chains.

5. Conclusion

A new zirconium diphosphonate fluoride has been prepared and characterized. Its structure has been solved ab initio by X-ray powder data from a conventional Bragg–Brentano diffractometer. This study confirms the potential of this technique for structural investigations of insoluble compounds or for studies when single-crystals are not available.

Investigation on zirconium *R*-amino-*N*,*N*-bis methylphosphonates started some years ago with the aim of finding a new layered structure with a poorly hindered interlayer region, with a free area per each organic group larger than those of α- and γ-zirconium phosphonate structures (about 24 and 36 Å^2, respectively). These studies allowed the preparation of a series of alkyl diphosphonate derivatives with a common layer framework. Now we have also found that considerably changing the nature of the *R* group, a compound with the same layer framework was formed. It is likely that many other hybrid inorgano-organic derivatives can be similarly prepared.

In this layer framework, the large free area potentially available for each organic group is doubly occupied by two interdigitated moieties. Future investigation will be devoted to finding out whether the whole space could be recovered to accommodate larger functional groups.

Acknowledgements

The authors wish to thank Prof. Pier Francesco Zanazzi for single crystal data collection and for useful discussions and suggestions. Funds by M.I.U.R. under the Project F.I.R.B. No. RBNE017MB5.

References

[1] G. Alberti, in: G. Alberti, T. Bein (Eds.), Comprehensive Supramolecular Chemistry, vol. 7, Pergamon Press, Oxford, 1996 (chapter 5).
[2] A. Clearfield, U. Costantino, in: G. Alberti, T. Bein (Eds.), Comprehensive Supramolecular Chemistry, vol. 7, Pergamon Press, Oxford, 1996 (chapter 4).
[3] A. Clearfield, in: K.D. Karlin (Ed.), Progress in Inorganic Chemistry, vol. 47, Wiley, New York, 1998, pp. 374–510.
[4] G. Alberti, M. Casciola, U. Costantino, R. Vivani, Adv. Mater. 8 (1996) 291–303.
[5] L.A. Vermeulen, R.Z. Fateen, P.D. Robinson, Inorg. Chem. 41 (2002) 2310–2312.
[6] D.M. Poojary, B. Zhang, A. Clearfield, Angew. Chem. Int. Ed. Engl. 33 (1994) 2324.

[7] A. Turner, P.A. Jaffres, E.J. MacLean, D. Villemin, V. McKee, G.B. Hix, J. Chem. Soc. Dalton Trans. (2003) 1314–1319.
[8] N. Stock, Solid State Sci 4 (2002) 1089–1094.
[9] J.-G. Mao, Z. Wang, A. Clearfield, Inorg. Chem. 41 (2002) 2334–2340.
[10] J.-G. Mao, Z. Wang, A. Clearfield, Inorg. Chem. 41 (2002) 3713–3720.
[11] J.-G. Mao, Z. Wang, A. Clearfield, Inorg. Chem. 41 (2002) 6106–6111.
[12] J.-G. Mao, Z. Wang, A. Clearfield, J. Chem. Soc. Dalton Trans. (2002) 4457–4463.
[13] H. Jankovics, M. Daskalakis, C.P. Raptopulou, A. Terzis, V. Tangoulis, J. Giapintzakis, T. Kiss, A. Salifoglou, Inorg. Chem. 41 (2002) 3366–3374.
[14] J.-L. Song, J.-G. Mao, Y.-Q. Sun, A. Clearfield, Eur. J. Inorg. Chem. (2003) 4218–4226.
[15] Z.-M. Sun, B.-P. Yang, Y.-Q. Sun, J.-G. Mao, A. Clearfield, J. Solid State Chem. 176 (2003) 62–68.
[16] U. Costantino, M. Nocchetti, R. Vivani, J. Am. Chem. Soc. 124 (2002) 8428–8434.
[17] R. Vivani, U. Costantino, M. Nocchetti, J. Mater. Chem. 12 (2002) 3254–3260.
[18] K. Moedritzer, A. Irani, J. Org. Chem. 31 (1966) 1603.
[19] A. Altomare, M.C. Burla, M. Camalli, G.L. Cascarano, C. Giacovazzo, A. Guagliardi, A.G.G. Moliterni, G. Polidori, R. Spagna, J. Appl. Crystallogr. 32 (1999) 115–119.
[20] G.M. Sheldrick, SHELXL-97, Program for the Refinement of Crystal Structures, University of Göttingen, Germany, 1997.
[21] P.E. Werner, L. Eriksson, M. Westdhal, J. Appl. Crystallogr. 18 (1985) 367–370.
[22] A. Boultif, D. Louer, J. Appl. Crystallogr. 24 (1991) 987–993.
[23] P.M. de Wolff, J. Appl. Crystallogr. 1 (1968) 108–113.
[24] J. Laugier, B. Bochu, LMGP-Suite, ENSP/Laboratoire des Matériaux et du Génie Physique, BP 46. 38042 Saint Martin d'Hères, France.
[25] V. Favre-Nicolin, R. Cerny, J. Appl. Crystallogr. 35 (2002) 734–743.
[26] M. Falcioni, M.W. Deem, J. Chem. Phys. 110 (1999) 1754–1766.
[27] A.C. Larson, R.B. von Dreele, Generalized Structure Analysis System, Los Alamos National Laboratory, NM, 2001.
[28] P. Thompson, D.E. Cox, J.B. Hastings, J. Appl. Crystallogr. 20 (1987) 79–83.
[29] L.W. Finger, D.E. Cox, A.P. Jephcoat, J. Appl. Crystallogr. 27 (1994) 892–900.